NASA Contractor Report 191024

On the Structure of Nonlinear Constitutive Equations for Fiber Reinforced Composites

Stefan Jansson
University of California
Santa Barbara, California

September 1992

Prepared for
Lewis Research Center
Under Grant NAG3–894

NASA
National Aeronautics and Space Administration

ON THE STRUCTURE OF NONLINEAR CONSTITUTIVE EQUATIONS FOR FIBER REINFORCED COMPOSITES

by
Stefan Jansson

Department of Mechanical and Environmental Engineering
University of California
Santa Barbara, California 93106

ABSTRACT

The structure of constitutive equations for nonlinear multiaxial behavior of transversely isotropic fiber reinforced metal matrix composites subjected to proportional loading has been investigated. Results from an experimental program have been combined with numerical simulations of the composite behavior for complex stress states to reveal the full structure of the equations. It was found that the nonlinear response can be described by a quadratic flow-potential, based on the polynomial stress invariants, together with a hardening rule that is dominated by two different hardening mechanisms.

INTRODUCTION

Useful constitutive equations are given by the simplest expression that can model an observed behavior with a desired accuracy. Various aspects are stressed in different applications. In the initial conceptual design stage convenience is more important than precise prediction and simple expressions are used for scoping calculations. However, more accurate descriptions are required in the later stages of the design to optimize and verify the performance of the structures. The latter type will be addressed here. Metal matrix composites (MMC's) reinforced with continuous ceramic fibers are strong and stiff, with only a weak nonlinearity in the response after matrix yield, when loaded in the fiber direction. In transverse tension and inplane shear the matrix carries a substantial part of the loading and the composite response is highly nonlinear when the matrix exhibits a nonlinear response. This strong anisotropic behavior imposes special requirements on the structure of the constitutive equations.

Hill's anisotropic yield surface has been used by fitting the free constants to a limited set of tests [Griffin et al, 1981] and [Bahei-El-Did et al, 1989]. The form of the yield surface is far too restrictive and the calculated responses are only valid for a very limited range of the stress space. Other constitutive equations are based on micro-mechanical models with simple assumptions of the local stress state in the composite; cf. [Aboudi,1982], [Min, 1981], and [Dovark and Bahei-El-Din, 1982]. Despite the simplifying

[Aboudi,1982], [Min, 1981], and [Dovark and Bahei-El-Din, 1982]. Despite the simplifying assumptions the resulting constitutive equations are quite lengthy and are unable to describe all essential features of the mechanical behavior with a sufficient accuracy. Detailed micro-mechanical models that include all the features of the composite behavior, cf. [Jansson, 1991], require numerical models that are of the same complexity as the structural problem. This implies that they are unsuitable for the analysis of structural problems because of the massive computational power required.

A continuum description of the composite behavior is a more powerful approach for the analysis of structural problems. Spencer [1988] formulated quite general constitutive equations for the case when the plastic deformation is inextensible in the fiber direction. Hashin et al [1974] assumed that the response in the fiber direction is elastic and that the transverse response is non-linear. Lou and Shapery [1971] assumed that the longitudinal strain in the matrix is governed by the fiber deformation, wheareas Robinson and Duffy [1990] assumed that the plastic deformation of the composite conserves volume. The in-plane response of a MMC has also been fitted to a quadratic flow-potential and an associated hardening law by Kenagat et al [1987]. Sun and Chen [1989] later noticed that this fit had too high of a longitudinal yield stress and effectively gave a linear elastic response in the longitudinal direction.

Many of the previous continuum formulations are extensions of constitutive equations developed for metals and assumptions appropriate for metals have been included in the formulation of the constitutive equations for the composites. These assumptions are far too restrictive for MMC's. In this paper the response of a detailed numerical model of a MMC will be used to provide guidance for the formulation of the constitutive equations. The model complements the experiments by providing responses for multiaxial stress states that would be difficult to achieve experimentally. It also has the advantage that the stress states can be selected so that the structure of the constitutive equations can be identified in a rational way.

OBSERVED MECHANICAL BEHAVIOR

The material used in this study is Du Pont's FP/AL [Campion et al., 1978]. It consists of continuous alumina fiber with a fiber diameter of approximately 20 Mn in uniaxial lay-up. The fiber volume fraction is 55% and the composite features a ductile Al-Li matrix with a strong fiber matrix bond. Mechanical properties have been reported by Jansson [1991].

The longitudinal tensile curve, Fig. 1a, has an initial linear response up to a stress of approximately 250 MPa, thereafter the matrix yields after which the slope of the curve shows a small decrease. The contraction in the transverse direction, Fig. 1b, is also linear up to matrix yield, when a small increase is observed.

The transverse tensile curve, Fig. 2a, has a linear response up to a stress of 75 MPa. The subsequent nonlinearity is much more pronounced than for the longitudinal loading. The ductility of 1% is low compared to the matrix ductility of 30%. The low ductility was attributed [Jansson, 1991] to high hydrostatic stresses that build up in the matrix during the plastic deformation and reduces the ductility of the matrix. The contraction in the other transverse direction, Fig. 2b, increases after matrix yield and tends to a slope of -1. The contraction in the fiber direction, Fig. 2c, decreases after matrix yield and tends to a very low rate.

Shear response for different shear loading are shown in Fig. 3. Inplane shear is given by the curves for $\alpha = 0°$ in Fig. 3, transverse shear is given by $\alpha = 90°$, and loading with equal components of inplane and transverse shear are given by $\alpha = 45°$. All the responses for the different loadings are very close and can be assumed to be identical. The difference is less than the variation observed between different samples. The failure strain in shear is close to the matrix ductility because high hydrostatic stresses do not build up [Jansson, 1991].

MODEL OF COMPOSITE MATERIAL

The fibers are randomly distributed in the transverse plane of the composite. In the analysis the fibers are assumed to be long parallel cylinders arranged in a hexagonal array, Fig 4a, with the fibers orientated in the 3-direction. A perfect bond is assumed between fiber and matrix. The hexagonal array is the periodical array with mechanical properties that have the closest symmetries to a transversely isotropic composite. They have identical transformation properties when the constituents are linear elastic. The hexagonal array has a deviation from transverse isotropy when the constituents have nonlinear responses, [Jansson, 1992]. The deviation is strongest for inplane shear. For the present volume fraction the shear loading τ_{13} cannot be expected to resemble the behavior of a composite with randomly distributed fibers because it activates slip on planes that are unconstrained by the fibers.

The theory of homogenization, cf. [Keller, 1976] and [Jansson, 1992], states that the macroscopic response of a periodical composite is governed by effective properties given by a boundary value problem on the unit cell when the wavelength of the macroscopic loading is long compared to the wavelength of the microstructure. The displacement field can then be written to a leading order as

$$u_i(x) = <\epsilon_{ij}> x_j + u_i^P(x) + u_i^0 \qquad (1)$$

where $<\epsilon_{ij}>$ is the global average strain giving rise to a constant displacement field on the unit cell, u^o_i is an arbitrary constant displacement, and u_i^P is a periodic displacement field that is equal on opposite sides of the unit cell. The macroscopic stress can be calculated from the local stress distribution in the unit cell as:

$$<\sigma_{ij}> = \frac{1}{V}\int_V \sigma_{ij}(x)dv \qquad (2)$$

The effective stress-strain response for the composite is determined by giving the average strain as input. The periodical displacement field and the local stress distribution are solved for and the effective stress is determined by use of eq. (2). All the considered stress states are symmetric or anti-symmetric with respect to the y_1 and y_2 axis, shown in Fig. 4a. The periodical displacement field has an inversion symmetry at the point ($y_1 = b/3/2$, $y_2 = b/2$). This implies that only an eighth of the indicated unit cell in Fig. 4a need be analyzed. The fibers are assumed to be linear-elastic and the matrix response is given by an elasto-plastic J_2 power law hardening rule. Because of material nonlinearity and complex geometry the finite element method has been used to solve the problem of the unit cell. The mesh is shown in Fig. 4b. The numerical procedure and boundary conditions are fully described in [Jansson, 1992].

It was found by Jansson, [1991] that the calculated responses agree well with the experimental observations for a matrix with an initial yield stress of 75 Mpa and a hardening exponent of 5. From Figs. 1-3 it can be deduced that the model exhibits all the features of the observed mechanical behavior of the composite.

CONSTITUTIVE EQUATIONS FOR COMPOSITE

General Structure

The total strain for the composite is assumed to be decomposed into a linear elastic and a nonlinear plastic part according to

$$d\epsilon_{ij} = d\epsilon^{e}_{ij} + d\epsilon^{p}_{ij} \qquad (3)$$

The elastic part is given as

$$\epsilon^{e}_{ij} = C_{ijkl}\sigma_{kl} \qquad (4)$$

where the compliance tensor C_{ijkl} has the symmetry properties of a transversely isotropic material, that is given by five independent constants. As mentioned earlier the inplane and transverse shear moduli are close and can be assumed to be equal and this reduces the number of constants to four. The plastic strain will be assumed to be given by a flow potential

$$d\epsilon_{ij}^{p}=\frac{\partial F}{\partial \sigma_{ij}}d\lambda \qquad (5)$$

with $d\lambda$ as a plastic multiplier. The remaining part of the paper will address the form of the flow potential F and the structure of the hardening rules that is required to exhibit the observed and computed behavior of the composite.

Formulation of Flow Potential

The yield surface is frequently used as a flow potential in plasticity theories and provides advantageous features such as stability and variational formulations. The shape of the initial yield surface for the composite was calculated by Jansson [1991]. Intersections of the yield surface and a plane orientated in the σ_{33} direction and at an angle φ with the σ_{11}- direction is shown in Fig. 5 where σ_{ym} is the initial yield stress of the matrix. Experimental results confirmed the general dimensions of the surface but the data points were not sufficiently close to give the detailed shape. The calculated surface is convex and can be described closely by a quadratic polynomial in the stress components for all stress states except close to $\sigma_{11} = -\sigma_{22}$ for which it has a sharp ridge. A ridge can be modeled by letting the surface be homogeneous in a non-integer exponent [Hill, 1979]. For a material exhibiting isotropic work hardening, the yield surface expands with a self-similar shape and surfaces for a constant amount of dissipated plastic work have self-similar shapes. Numerically calculated surfaces in the σ_{11}-σ_{22} plane are shown in Fig. 6 for different amounts of dissipated plastic work (W_p). The surface with zero dissipated energy is the initial yield surface. The sharp corners of the initial yield surface disappear after a small amount of plastic dissipation. The subsequent shape is smooth and the expansion is nonuniform with faster growth in the $\sigma_{11} = \sigma_{22}$ direction than in the $\sigma_{11} = -\sigma_{22}$ direction.

The transition regime between the surface with sharp corners to the smooth surface is short and does not justify the complexity that would be required to include this transition. Disregarding the corner, the surface can then be approximated by a quadratic polynomial in the stress components. The polynomial invariants of the stress tensor for a transversely isotropic material, cf. Green and Adkins [1960], are

$$\sigma_{11}+\sigma_{22};\ \sigma_{33};\ \frac{1}{4}(\sigma_{11}-\sigma_{22})^2+\sigma_{12}^2;,\ \sigma_{13}^2+\sigma_{23}^2;\ |\sigma_{ij}|$$

when the symmetry axis is orientated in the 3-direction and the symmetry $\sigma_{ij} = \sigma_{ji}$ of the stress tensor has been used. This set of invariants is not unique but irreducible. The present form is the most convenient for the formulation of constitutive equations because the different invariants can be directly associated with different loadings. Including terms up to second order gives the following polynomial in the stress invariants;

$$F \equiv \left[\frac{\sigma_{11}+\sigma_{22}}{K_T}\right]^2 + \left[\frac{\sigma_{33}}{K_L}\right]^2 - \frac{(\sigma_{11}+\sigma_{22})\sigma_{33}}{K_{LT}^2} + \frac{(\sigma_{11}-\sigma_{22})^2+4\sigma_{12}^2}{4K_{TS}^2} + \frac{\sigma_{13}^2+\sigma_{23}^2}{K_{IS}^2} \tag{6}$$

Letting

$$F-1=0 \tag{7}$$

for initial yielding; defines K_L as the longitudinal yield stress, $K_T/2$ as the yield stress for transverse biaxial tension; K_{TS} as the yield stress in transverse shear; K_{IS} as the yield stress in inplane shear; and K_{LT} to be a constant defining the interaction of combined longitudinal and transverse loading. Convexity of the surface requires the negative sign in front of the interaction term together with the condition

$$K_{LT}^2 > \frac{K_L K_T}{2} \tag{8}$$

The plastic strain components are normal to the flow potential and are given by eq. (5) where $d\lambda$ is the plastic multiplier whose magnitude is governed by the hardening function.

The suitability of using the surface F as the flow potential and the structure of hardening rules will be investigated using the stress-strain responses for different loading paths. The stress-strain relationships are generated by the numerical model that provide plastic strain increments and current stresses as output. The loadings paths have been selected such that ratios of the yield stresses $K(_i)$, that define the flow potential, can be determined conveniently in terms of strain increments and current stresses.

For example, the normality rule (5) gives the strain increments resulting from a tensile load applied in the 1-direction:

$$d\epsilon_{11}^p = \left[2\frac{\sigma_{11}}{K_T^2} + \frac{\sigma_{11}}{2K_{TS}^2}\right] d\lambda$$

$$d\epsilon_{22}^p = \left[\frac{\sigma_{11}}{K_T^2} - \frac{\sigma_{11}}{2K_{TS}^2}\right] d\lambda$$

Eliminating $d\lambda$ and solving for K_{TS}/K_T gives

$$\frac{K_{TS}}{K_T} = \frac{1}{2}\sqrt{\frac{d\epsilon^p_{11}+d\epsilon^p_{22}}{d\epsilon^p_{11}-d\epsilon^p_{22}}} \tag{9}$$

in terms of the plastic strain increments. Similar expressions have been derived for the other loading paths used in this study and are given in appendix A.

The general trends for the ratios of the calculated yield stresses are given in Figs. 7 - 10. In the following it is convenient to separate the loadings into an axi-symmetric part (with respect to the fiber orientation) that is given by the first three terms in the flow potential (6) and shear part that is given by the last two terms in (6). For axi-symmetric loading the ratios remain constant after a short initial transition period. The ratio given by the initial yield surface agrees very well for K_{LT}/K_L , Fig. 7, and is somewhat higher than the calculated steady state value for K_{LT}/K_T , Fig. 8.

The computations indicate that the interaction between inplane (σ_{13}, σ_{23}) and transverse shear (σ_{12}) is quadratic. This is also supported by the experimental observations given in Fig. 3. The other computed stress strain curves are given in Jansson [1992]. A quadratic interaction can be expected because local stress states in the composite are orthogonal and interaction through the matrix yield condition is quadratic.

Transverse tension is a combination of axi-symmetric biaxial tension ($\sigma_{11}=\sigma_{22}$) and transverse shear (σ_{12}) in the present formulation, cf. eq. (6) . This type of loading forms additional requirements on the evolution of the yield stresses. Ratios of the yield stresses defining the axi-symmetric part of the flow potential are given in Fig. 8 for transverse loading. The ratios attain a constant value after a short transition period and this is the same trend as for the axi-symmetric loading. Curiously the σ_{22} loading has a long transition period. A representative example of ratios of yield stress for axi-symmetric loading to yield stress for shear loading is given in Fig. 9. It indicates that the yield stresses for the axi-symmetric part initially increases much faster than the yield stress for shear loading. The ratios tends to an asymptotic value which is much lower than the one given by the initial yield surface.

It can be deduced that the normality requires that the ratios of the yield stresses defining the flow potential for axi-symmetric loading remain constant during the loading and are closely given by the initial yield surface. The ratio of the yield stresses for shear loading to yield stresses for axi-symmetric loading decrease gradually during the plastic deformation to saturation values that are significantly lower than the values given by the initial yield surface.

Hardening Rule

A frequently used hardening rule in metal plasticity is isotropic work hardening with a self-similar expansion of the yield surface. Applying a similar idea here the incremental plastic work is

$$dW^{P}=\sigma_{ij}d\epsilon^{P}_{ij} \tag{10}$$

The normality rule (5) gives relations of the incremental plastic strain components $d\epsilon_{ij}$ in terms of the stresses σ_{ij} and the plastic multiplier $d\lambda$. Inverting the relations to get expressions for the stresses in terms of the plastic strain components and substituting them into (10) gives the following expression for the incremental plastic work

$$dW^{P}=\left[\frac{2}{4-\left[\frac{K_L K_T}{K_{LT}^2}\right]^2}\left[\frac{K_t^2}{4}(d\epsilon^{P}_{11}+d\epsilon^{P}_{22})^2+K_L^2(d\epsilon^{P}_{33})^2+\frac{K_L^2K_T^2}{2K_{LTx}}(d\epsilon^{P}_{11}+d\epsilon^{P}_{22})d\epsilon^{P}_{33}\right]+\right.$$

$$\left.\frac{K_{TS}^2}{2}\left[(d\epsilon^{P}_{11}-d\epsilon^{P}_{22})^2+4(d\epsilon^{P}_{12})^2\right]+\frac{K_{IS}^2}{2}\left[(d\epsilon^{P}_{13})^2+(d\epsilon^{P}_{23})^2\right]\right]\frac{1}{d\lambda} \tag{11}$$

The requirement for positive dissipation is the same as the convexity condition (8), which is fulfilled by the initial yield surface. For isotropic hardening and proportional loading the plastic work may also be expressed as a function of a scalar equivalent plastic strain that can be identified from (11) as

$$(d\epsilon^{P}_{e})^2=\frac{2}{4-\left[\frac{K_L K_T}{K_{LT}^2}\right]^2}\left[\frac{K_t^2}{4}(d\epsilon^{P}_{11}+d\epsilon^{P}_{22})^2+K_L^2(d\epsilon^{P}_{33})^2+\frac{K_L^2K_T^2}{2K_{LT}^2}(d\epsilon^{P}_{11}+d\epsilon^{P}_{22})d\epsilon^{P}_{33}\right]+$$

$$\frac{K_{TS}^2}{2}\left[(d\epsilon^{P}_{11}-d\epsilon^{P}_{22})^2+4(d\epsilon^{P}_{12})^2\right]+\frac{K_{IS}^2}{2}\left[(d\epsilon^{P}_{13})^2+(d\epsilon^{P}_{23})^2\right] \tag{12}$$

For a material exhibiting isotropic work hardening values of the function F with constants K_i given by the initial yield surface and stresses σ_{ij} from different loadings will fall on one master curve when plotted as a function of the dissipated plastic work or the equivalent plastic strain. In Fig. 10 the value of F has been plotted versus the equivalent plastic strain for different loadings. It can be deduced that the results fall into three different groups of curves. One group consist of axi-symmetric loadings with respect to the fiber that also has the strongest hardening. The second group is given by the transverse and inplane shear loadings that has a weak hardening. The third group is given by the transverse tension that is a combination of axi-symmetric and shear loading and has an intermediate hardening. The results also indicate that pure hydrostatic loading causes the same magnitude of plastic strain as longitudinal tension. This implies that incompressibility should not be used as a constraint on the constitutive equations when the nonlinearity of the longitudinal response is included. This also leaves the freedom to fit the experimental observation better.

These observations suggest that the hardening function should be separated into two parts as

$$\frac{dK_T}{K_T^0}=\frac{dK_L}{K_L^0}=\frac{dK_{LT}}{K_{LT}^0}=H_A d\epsilon^{P}_{Ae} \tag{13a}$$

$$\frac{dK_S}{K_S^0}=H_S(\epsilon^{P}_{Se})d\epsilon^{P}_{Se} \tag{13b}$$

where the superscript o stands for the initial yield surface and the effective strains in the hardening functions are defined respectively as

$$(d\epsilon^{P}_{Ae})^2=\left[\frac{K_T}{2K_L}\right]^2(d\epsilon^{P}_{11}+d\epsilon^{P}_{22})^2+(d\epsilon^{P}_{33})^2+\frac{1}{2}\left[\frac{K_T}{K_{LT}}\right]^2(d\epsilon^{P}_{11}+d\epsilon^{P}_{22})d\epsilon^{P}_{33} \tag{14a}$$

$$(d\epsilon^{p}_{Se})^2=(d\epsilon^{p}_{12})^2+\frac{1}{4}(d\epsilon^{p}_{11}-d\epsilon^{p}_{22})^2+(d\epsilon^{p}_{13})^2+(d\epsilon^{p}_{23})^2 \qquad (14b)$$

The first equation (13a) gives the hardening for axi-symmetric loading and referring to Fig. 10 is assumed to be linear in the effective strain. It is dominated by the constraint induced by the stiff fiber and the results in Fig. 11 indicate that H_A is large. The second equation (13b) gives the hardening for shear loading and is highly nonlinear because the fibers constraints the shear loadings moderately. As stated earlier the inplane and transverse shear curves are close and can be assumed to be equal giving $K_{TS} = K_{IS} = K_S$.

It is obvious from the previous results that the flow rule, eq.(5), and the flow potential (6) together with the hardening rules, eq. (13), give excellent results for pure axi-symmetric or shear loading. It remains, to evaluate how well they describe the behavior under combinations of shear and axi-symmetric loadings. The value of the flow potential F has been plotted in Fig. 11a for different transverse loadings by using the hardening functions (13). The hardening functions have been determined from the axi-symmetric and shear responses given in Fig. 10. An exact fit requires the flow potential F to attain a constant value of unity throughout the deformation. It can be deduced from Fig. 11a that the hardening is not sufficiently strong to keep the value of F constant and equal to one, especially for stress states close to transverse biaxial tension.

This discrepancy can be overcome by introducing cross hardening terms in the hardening functions (13) with

$$\frac{dK_T}{K_T^0}=\frac{dK_L}{K_L^0}=\frac{dK_{LT}}{K_{LT}^0}=H_A d\epsilon^{p}_{Ae}+H_{AS}d\epsilon^{p}_{Se} \qquad (15a)$$

$$\frac{dK_S}{K_S^0}=H(\epsilon^{p}_{Se})d\epsilon_{Sesp}+H_{SA}d\epsilon^{P}_{Ae} \qquad (15b)$$

where the cross hardenings have been assumed to be linear in the effective strains for simplicity. A cross hardening of $H_{SA} = 0.2H_A$ in the shear hardening causes the value of F to remain constant, Fig. 11b. This effect can also be established by a cross-hardening of $H_{AS} = 30\ H_A$ in the axi-symmetric hardening, Fig. 11c.

The most preferable of the two cross hardenings is the one that gives the closest trend to that required by the normality shown in Fig. 9. The history of K_S/K_T with no cross hardening is given in Fig. 12a. A cross-term in the shear hardening causes the ratio

to decrease more slowly, as indicated in Fig. 12b, while a cross-term in the axi-symmetric hardening causes the ratio to decrease faster, Fig 12c. A comparison of the results in Figs. 12a-c with Fig. 9 indicate that the axi-symmetric hardening has the most appreciable affect when a single cross hardening term is used.

DETERMINATION OF CONSTANTS

A longitudinal tensile test provides the initial yield stress K_L° and the interaction constant K_{LT}° is given through the transverse contraction as shown by the relation

$$K_{LT}^0 = K_L^0 \sqrt{-\frac{2d\epsilon_{33}^p}{d\epsilon_{11}^p}} \tag{16}$$

derived from the normality condition. The constant H_A in the axi-symmetric hardening function can thereafter be determined from the longitudinal tests as

$$H_A = \frac{d\sigma_{33}}{\sqrt{(K_{LT}^0)^2 d\epsilon_{11}^p + (K_L^0)^2 d\epsilon_{33}^p}} \tag{17}$$

The inplane shear tests provides the initial yield stress K_s^0 and the nonlinear shear hardening slope $H_S(\epsilon_{Se}^p)$.

The initial yield stress for transverse biaxial tension can now be determined from the transverse tensile test by use of the initial yield stress in shear as

$$K_T^0 = \frac{2K_S^0 \sigma_T^0}{\sqrt{4(K_S^0)^2 - (\sigma_T^0)^2}} \tag{18}$$

where σ_T° is the initial yield stress in transverse tension. The values of the initial yield stresses are restricted by the requirement of positive dissipation (8) and the initial yield stress for transverse biaxial tension is also higher than the initial yield stress in shear.

The cross-hardening term H_{SA} can be estimated from the transverse stress strain curve by satisfying the yield condition close to saturation. This calculation gives the relationship

$$H_{SA}=\left[\frac{K_s}{K_s^0}-\int_0^{\epsilon_{se}^p} H(\epsilon)d\epsilon\right]\frac{1}{\epsilon_{Ae}^p} \tag{19}$$

where

$$K_S=\frac{1}{2}\left[\frac{1}{\sigma_T^2}-\frac{1}{K_T^2}\right]^{-\frac{1}{2}} \tag{20}$$

The other cross-hardening term H_{AS} has a strong effect on the contraction in the unloaded transverse direction and can be included when it is appreciable.

The constitutive equations include many constants and a direct systematic determination of the constants cannot be expected to give the best possible description of the mechanical behavior. The response have to be evaluated and compared with the experimental data for the different loadings. It is likely that the description can be improved by adjusting some of the constants. Experience has shown that the best fit is usually obtained by using interactive computer graphics to display the results and a human link in the loop to make the final adjustments.

CONCLUSIONS

It was found that a quadratic flow potential based on the polynomial stress invariants can be used to describe the mechanical behavior of fiber reinforced composite subjected to proportional loading. This formulation requires that the hardening function is separated into two parts: a strong linear hardening for axi-symmetric loading, that is dominated by the stiff fiber, and a weak nonlinear hardening, that is dominated by the matrix, for the inplane and transverse shear loadings. Calculations and experiments indicate that the composite can be assumed to have identical responses for the two shear loadings.

Cross-terms in the hardening functions improves the accuracy for transverse tension by increasing the hardening and rate of constraint in the fiber. The cross-hardening can be neglected if an error of 20 % in stress can be accepted in transverse tensile or shear response.

The plastic strain components for longitudinal tension and hydrostatic loading are of the same order. Hence, a consistent simplification of the constitutive equations is to assume inextensibility in the longitudinal direction when the plastic deformation is assumed to be incompressible. This assumption makes the constitutive equations

particularly easy and suitable for hand calculations. It implies that the composite can only deform in inplane and transverse shear.

In a subsequent paper these constitutive equations will be implemented into a general finite element program and the performance of the equations will be evaluated for representative structural components.

ACKNOWLEDGEMENT

This work was supported by grants from Sandia National Laboratories and the NASA-Lewis Research Center.

REFERENCES

Aboudi, J., 1982, "A Continuum Theory for Fiber-Reinforced Elastic-Viscoplastic Composites," International Journal of Engineering Science, vol. 20, pp. 605-621.

Bahel-El-Din, Y. A., Dvorak, G. J., and Wu, J., 1989, "Fracture of Fibrous Metal Matrix Composites - II. Modeling and Numerical Analysis," Engineering Fracture Mechanics, vol. 34, pp.105-123.

Green, A. H. and Adkins, J. E. 1960, Large Elastic Deformations, Claredon Press, Oxford.

Griffin, O. H., Kamat, M. P., and Herakovich, C. T., 1981, "Three-Dimensional Finite Element Analysis of Laminated Composites," Journal of Composite Materials, vol. 5, pp. 543-560.

Hashin, Z., Bagehl, D., and Rosen, B. W., 1974, "Non-Linear Behavior of Fiber Composite Laminates," NASA CR-2313, 130 pp.

Hill. R., 1979, "Theoretical Plasticity of Textured Aggregates," Mathematical Proceedings of Cambridge Philosophical Society, vol. 85, pp. 179-191.

Jansson, S. 1991, " Mechanical Characterization and Numerical Modeling of Nonlinear Deformation and Fracture of a Fiber Reinforced Metal Matrix Composite," Mechanics of Materials, vol. 12, pp. 47-62.

Jansson, S. 1992, "Homogenized Nonlinear Constitutive Properties and Local Stress Concentrations for Composites with Periodic Internal Structure," International Journal of Solids and Structures, vol. 29., no. 17, pp. 2181-2200.

Keller, J. B., 1976, "Effective Behaviour of Hetrogeneous Media," in: Statistical Mechanics and Statistical Methods in Iheory and Application, U. Landman Ed., Plenum Press, New Yourk.

Kenaga, D., Doely, J. F., and Sun, C. T., 1987, "The Characterization of Boron/Aluminum Composite in the Nonlinear range as an Orthotropic Elasto-plastic Material," Journal of Composite Materials, vol. 21, pp. 516-529.

Lou, Y. C. and Shapery, R. A., 1971, "Viscoelastic Characterization of a Nonlinear Fiber-Reinforced Plastic," Journal of Composite Materials, vol. 5, pp. 208-234.

Min, B. K., 1981, "A Plane Stress Formulation for Elastic-plastic Deformation of Unidirectional Composites," Journal of the Mechanics and Physics of Solids, vol. 29, pp. 327-352.

Robinson, D. N. and Duffy, S. F., 1990, "A Continuum Deformation Theory for Metal-Matrix Composites at High Temperature," ASCE Journal of Engineering Mechanics, vol. 116, pp. 832-844.

Spencer, A. J. M., 1988, "Yield Conditions and Hardening Rules for Fiber-Reinforced Materials with Plastic Response," University of Nottingham Report.

Sun,C. T. and Chen, J. L., 1989, "A Simple flow Rule for Characterizing Nonlinear Behavior of Fiber Composites, " Journal of Composite Materials, vol. 23, pp. 1009-1020.

APPENDIX A

Longitudinal tension

$\sigma_{33} \neq 0$

$$d\epsilon^{p}_{33} = 2\frac{\sigma_{33}}{K_L^2} d\lambda \tag{A.1}$$

$$d\epsilon^{p}_{11} = d\epsilon^{p}_{22} = -\frac{\sigma_{33}}{K_{LT}^2} d\lambda \tag{A.2}$$

gives

$$\frac{K_{LT}}{K_L} = \sqrt{-\frac{d\epsilon^{p}_{33}}{2d\epsilon^{p}_{11}}} \tag{A.3}$$

Transverse biaxial tension and longitudinal plane strain

$\sigma_{11} = \sigma_{22}$, $d\epsilon^{p}_{33} = 0$

$$d\epsilon^{p}_{33} = \left[2\frac{\sigma_{33}}{K_L^2} - \frac{\sigma_{11}+\sigma_{22}}{K_{LT}^2}\right] d\lambda = 0 \tag{A.4}$$

gives

$$\frac{K_{LT}}{K_L} = \sqrt{\frac{\sigma_{11}}{\sigma_{33}}} \tag{A.5}$$

Transverse biaxial tension

$\sigma_{11}=\sigma_{22}$

$$d\epsilon^{p}_{11}=d\epsilon^{p}_{22}=2\frac{\sigma_{11}+\sigma_{22}}{K_T^2}d\lambda \tag{A.6}$$

$$d\epsilon^{p}_{33}=-\frac{\sigma_{11}+\sigma_{22}}{K_{LT}^2}d\lambda \tag{A.7}$$

gives

$$\frac{K_{LT}}{K_T}=\sqrt{-\frac{d\epsilon^{p}_{11}}{2d\epsilon^{p}_{33}}} \tag{A.8}$$

Longitudinal tension and transverse plane strain

σ_{33}, $d\epsilon^{p}_{11}=d\epsilon^{p}_{22}=0$ **(40)**

$$d\epsilon^{p}_{11}=d\epsilon^{p}_{22}=\left[2\frac{\sigma_{11}+\sigma_{22}}{K_T^2}-\frac{\sigma_{33}}{K_{LT}^2}\right]d\lambda=0 \tag{A.9}$$

gives

$$\frac{K_{LT}}{K_T}=\sqrt{\frac{\sigma_{33}}{4\sigma_{11}}} \tag{A.10}$$

Transverse tension

$\sigma_{11} \neq 0$

$$d\epsilon^{p}_{11} = \left[2\frac{\sigma_{11}}{K_T^2} + \frac{\sigma_{11}}{2K_{TS}^2} \right] d\lambda \tag{A.11}$$

$$d\epsilon^{p}_{22} = \left[2\frac{\sigma_{11}}{K_T^2} - \frac{\sigma_{11}}{2K_{TS}^2} \right] d\lambda \tag{A.12}$$

$$d\epsilon^{p}_{33} = -\frac{\sigma_{11}}{K_{LT}^2} d\lambda \tag{A.13}$$

gives

$$\frac{K_{TS}}{K_L} = \frac{1}{2}\sqrt{\frac{d\epsilon^{p}_{11} + d\epsilon^{p}_{22}}{d\epsilon^{p}_{11} - d\epsilon^{p}_{22}}} \tag{A.14}$$

$$\frac{K_{LT}}{K_T} = \frac{1}{2}\sqrt{-\frac{d\epsilon^{p}_{11} + d\epsilon^{p}_{22}}{d\epsilon^{p}_{33}}} \tag{A.15}$$

Transverse loading close to biaxial tension

$$d\epsilon^{p}_{22} = -\frac{d\epsilon^{p}_{11}}{4}$$

gives

$$\frac{K_{TS}}{K_T} = \sqrt{\frac{3}{20}\frac{\sigma_{11}-\sigma_{22}}{\sigma_{11}+\sigma_{22}}} \tag{A.16}$$

$$\frac{K_{LT}}{K_T} = \frac{1}{2}\sqrt{-\frac{d\epsilon^{p}_{11}+d\epsilon^{p}_{22}}{d\epsilon^{p}_{33}}} \tag{A.17}$$

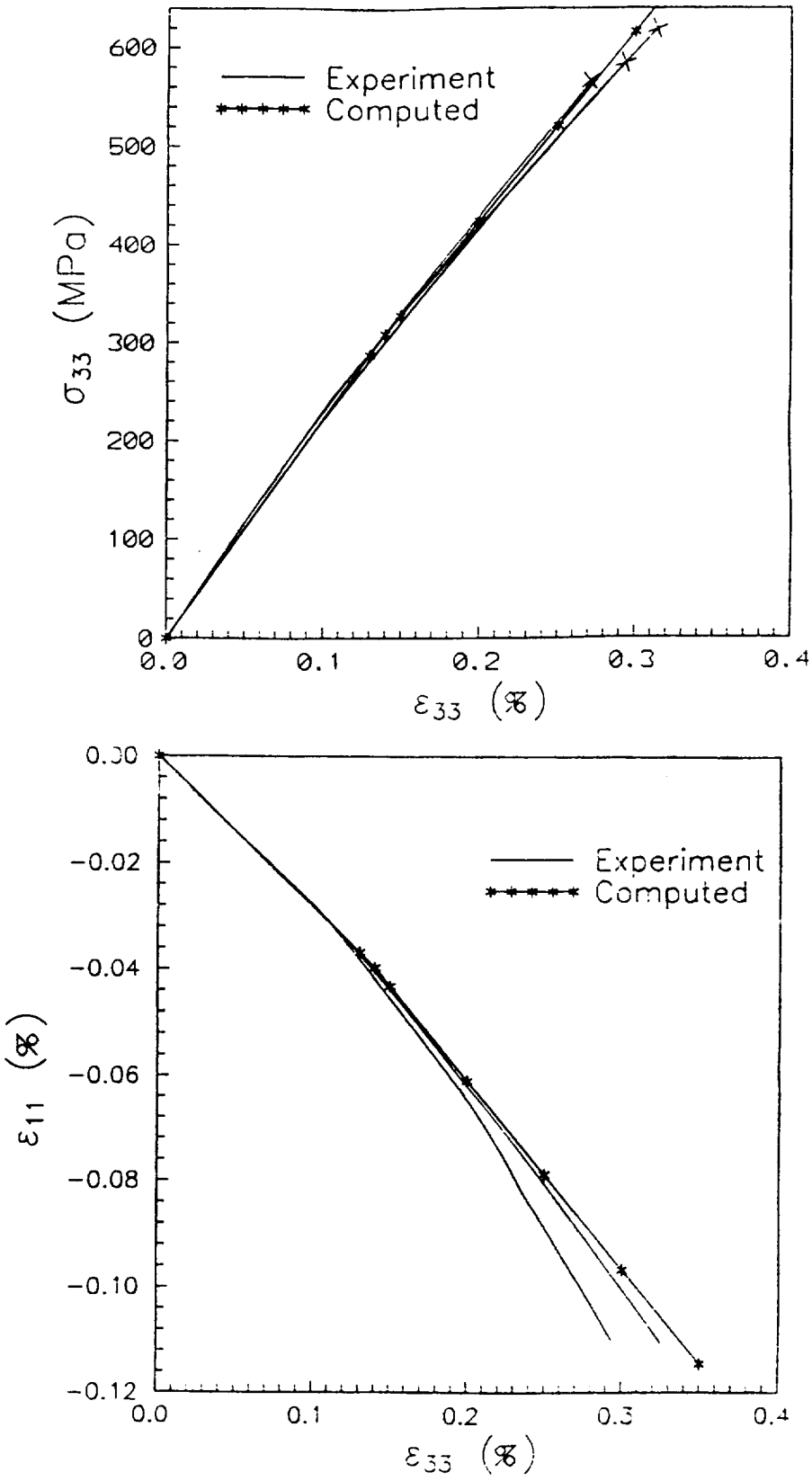

Fig. 1 Longitudinal tension. a) tensile curve, b) transverse contraction

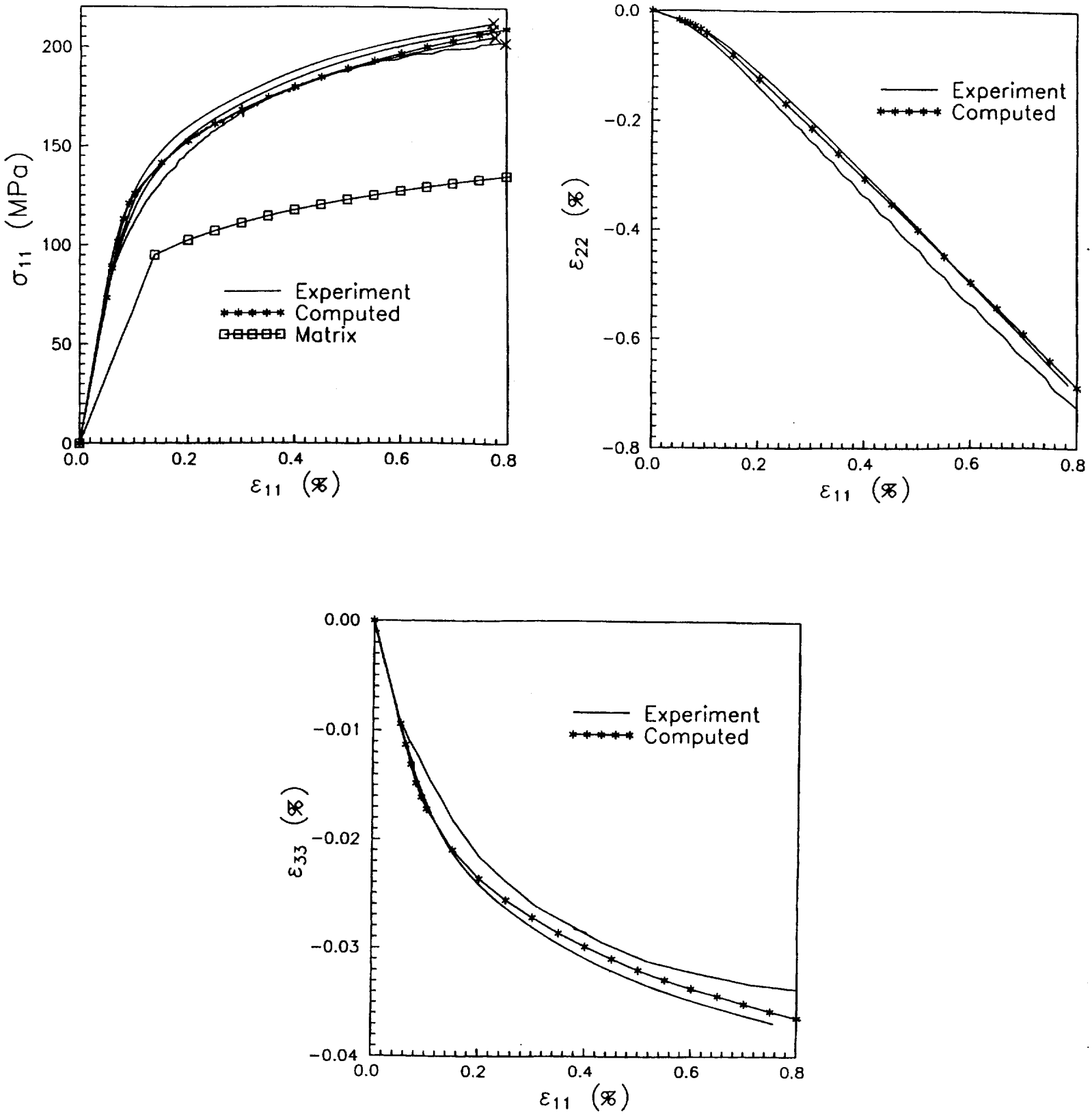

Fig. 2 Transverse tension. a) tensile curve, b) contraction in other transverse direction, c) contraction in longitudinal direction.

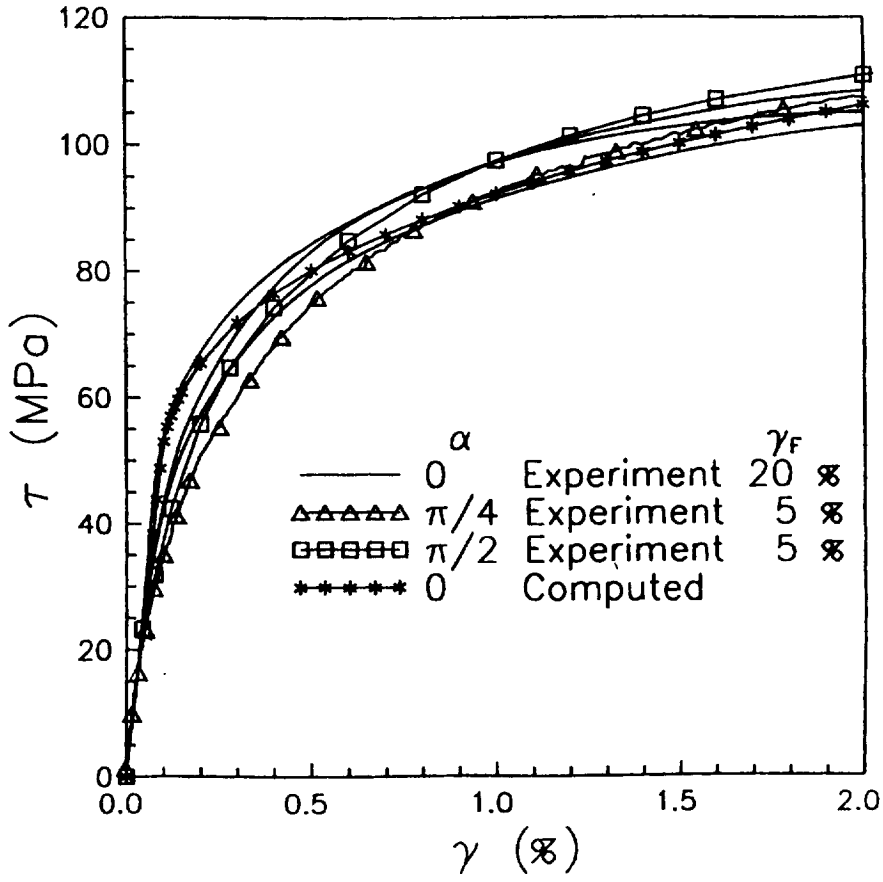

Fig. 3 Shear loading. Inplane shear $\alpha = 0$, transverse shear $\alpha = \pi/2$, and $\alpha = \pi/4$ equal components of inplane and transverse shear.

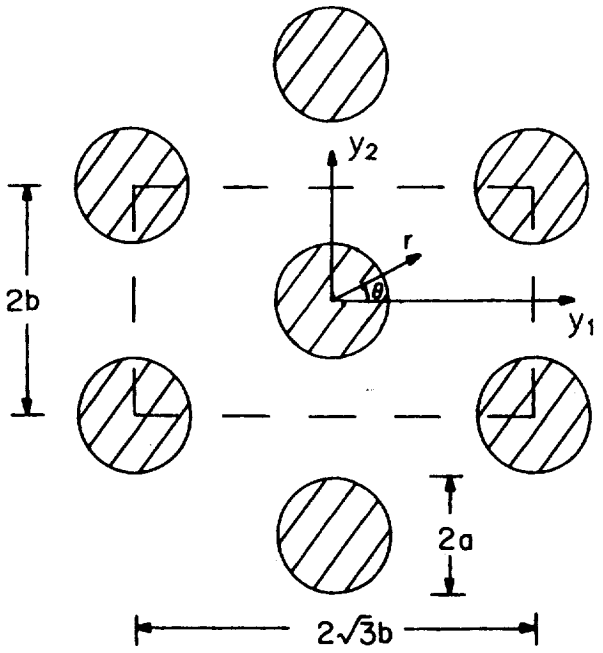

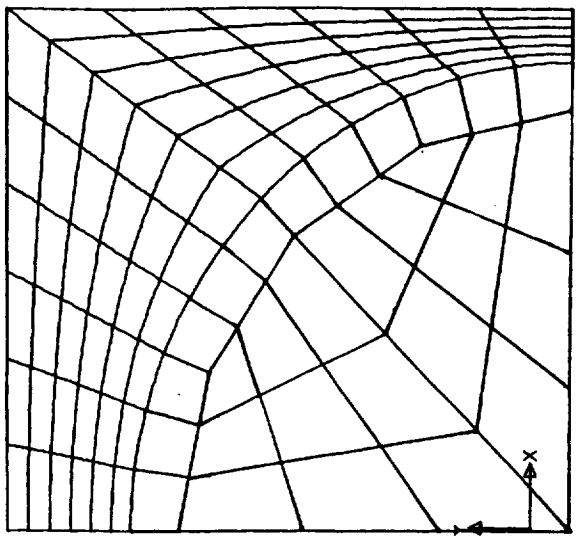

Fig. 4 Model of composite. a) Hexagonal array, b) Finite element mesh of unit cell.

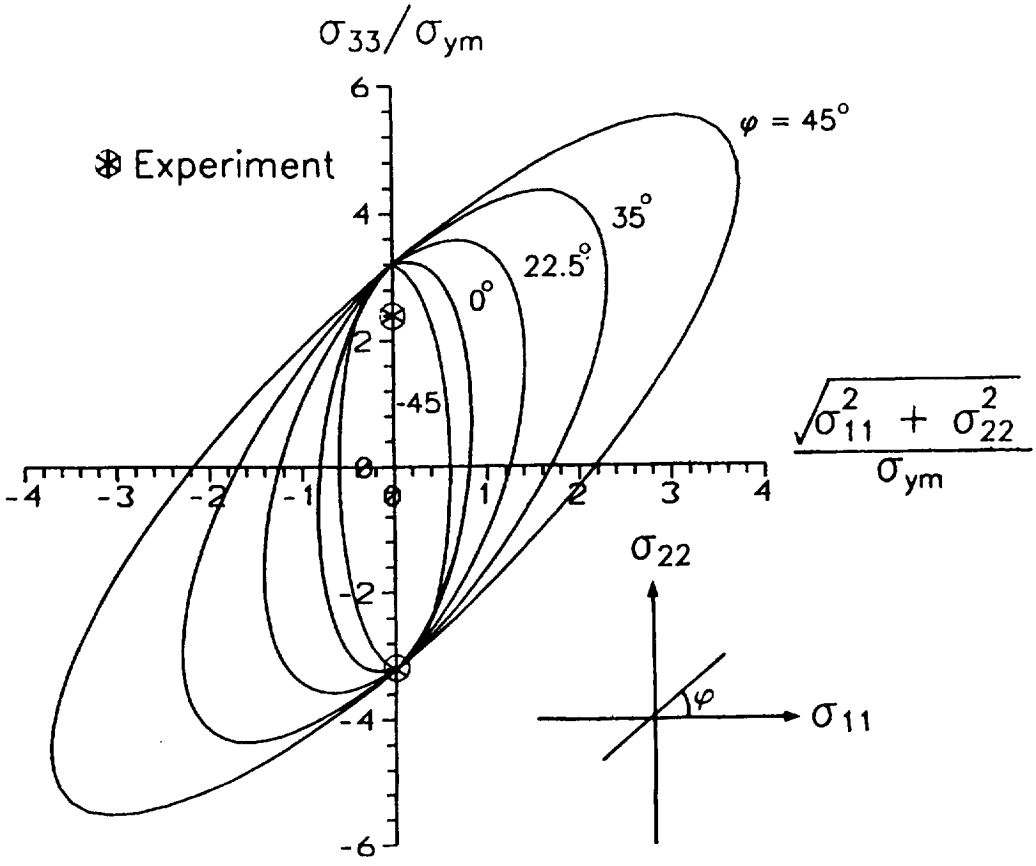

Fig. 5 Initial yield surface in the σ_{11}-σ_{22}-σ_{33} space.

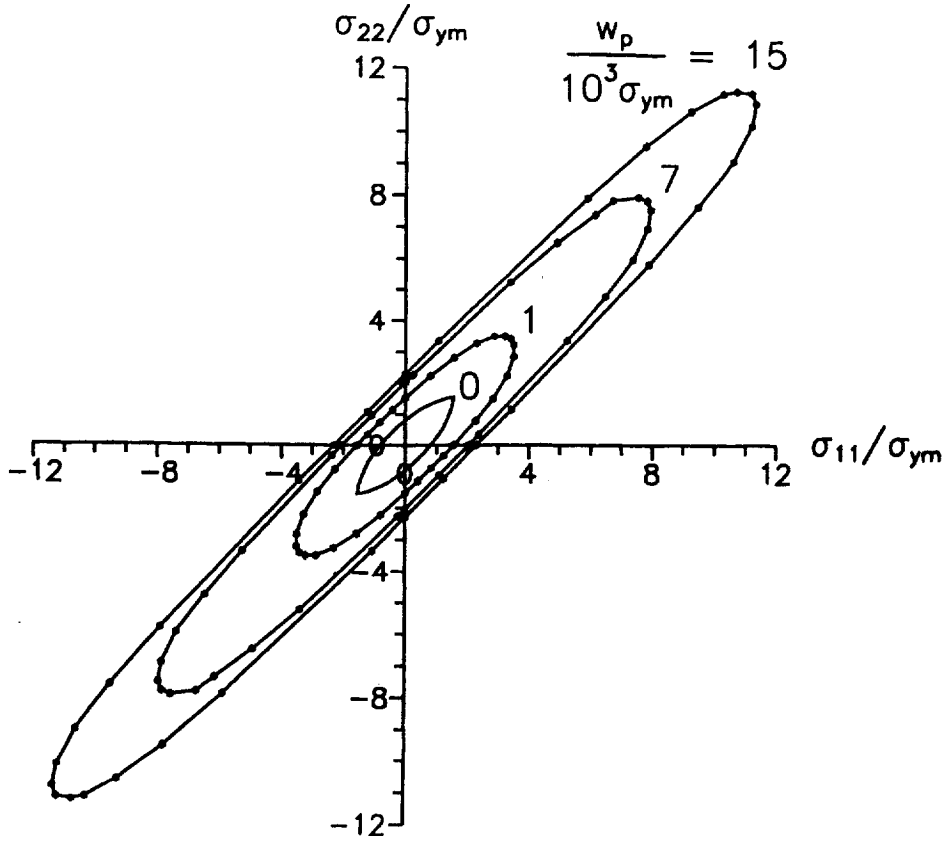

Fig. 6 Contours of constant dissipated energy in the σ_{11}-σ_{22} plane.

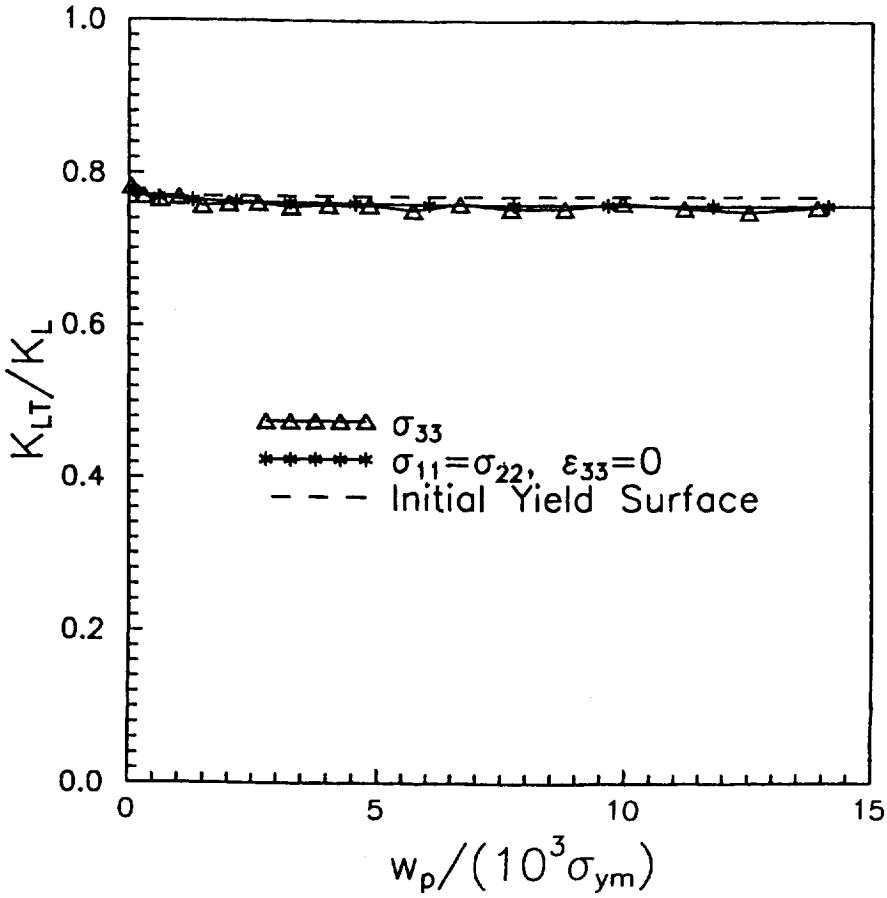

Fig. 7 Ratio of yield stresses for axi-symmetric part of flow-potential for axi-symmetric loading.

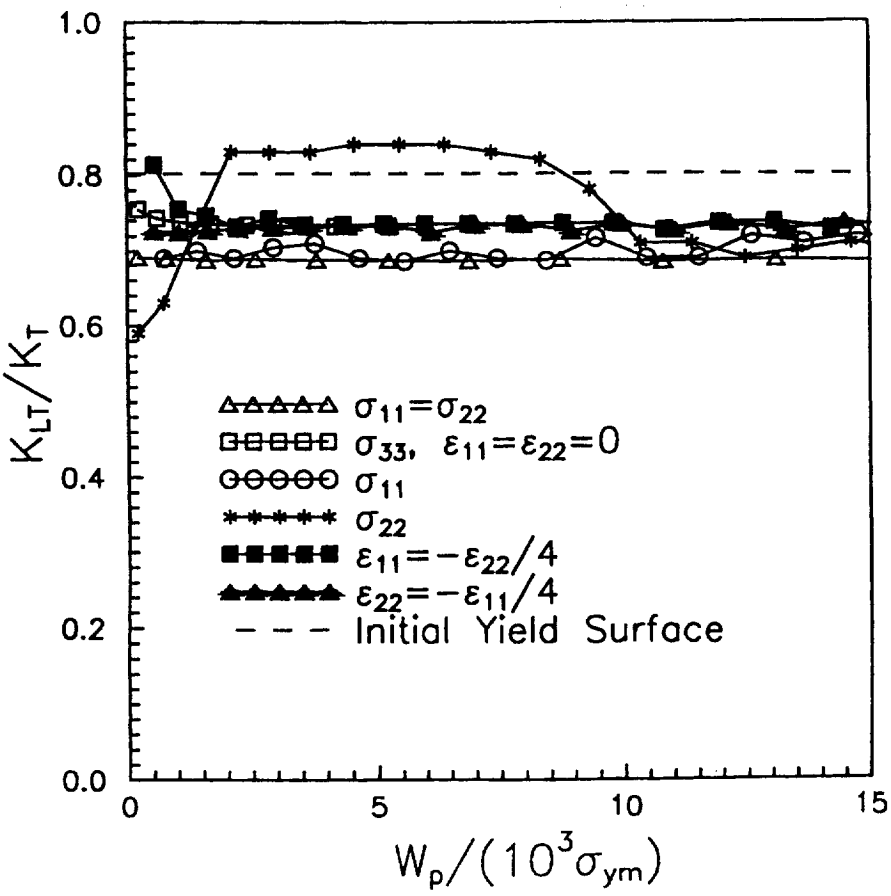

Fig. 8 Ratio of yield stresses for axi-symmetric part of flow-potential for axi-symmetric and combinations of axi-symmetric and shear loadings.

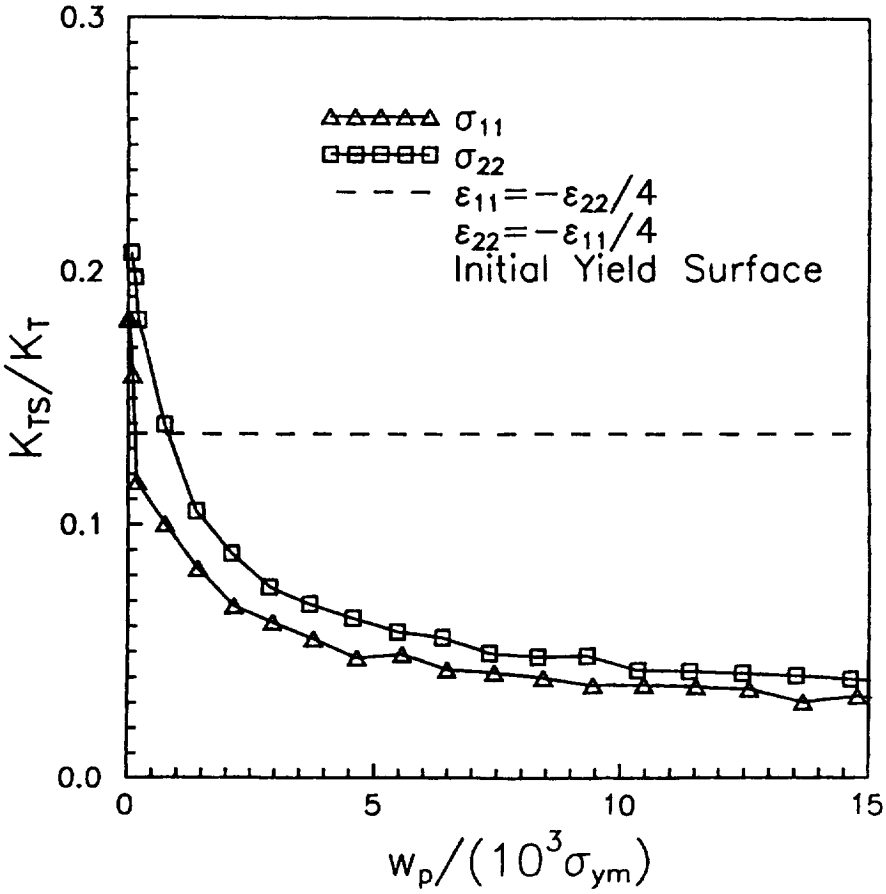

Fig. 9 Ratio of yield stresses for shear and axi-symmetric part of flow-potential for transverse loading.

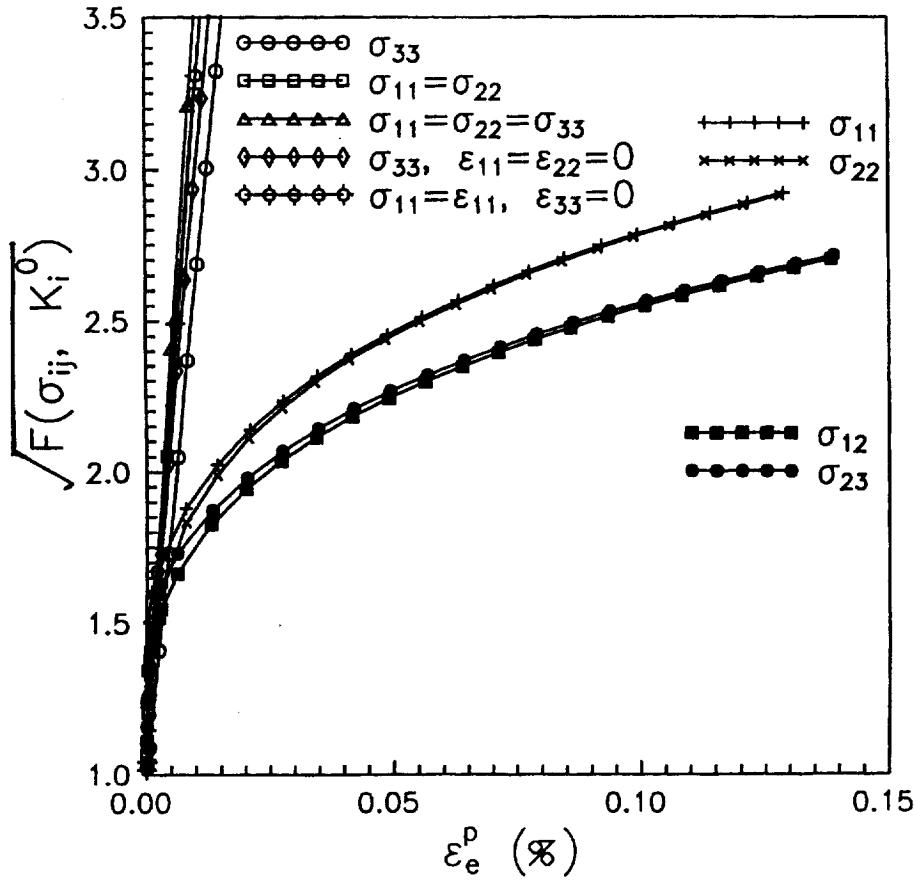

Fig. 10 Value of flow-potential for different loading paths.

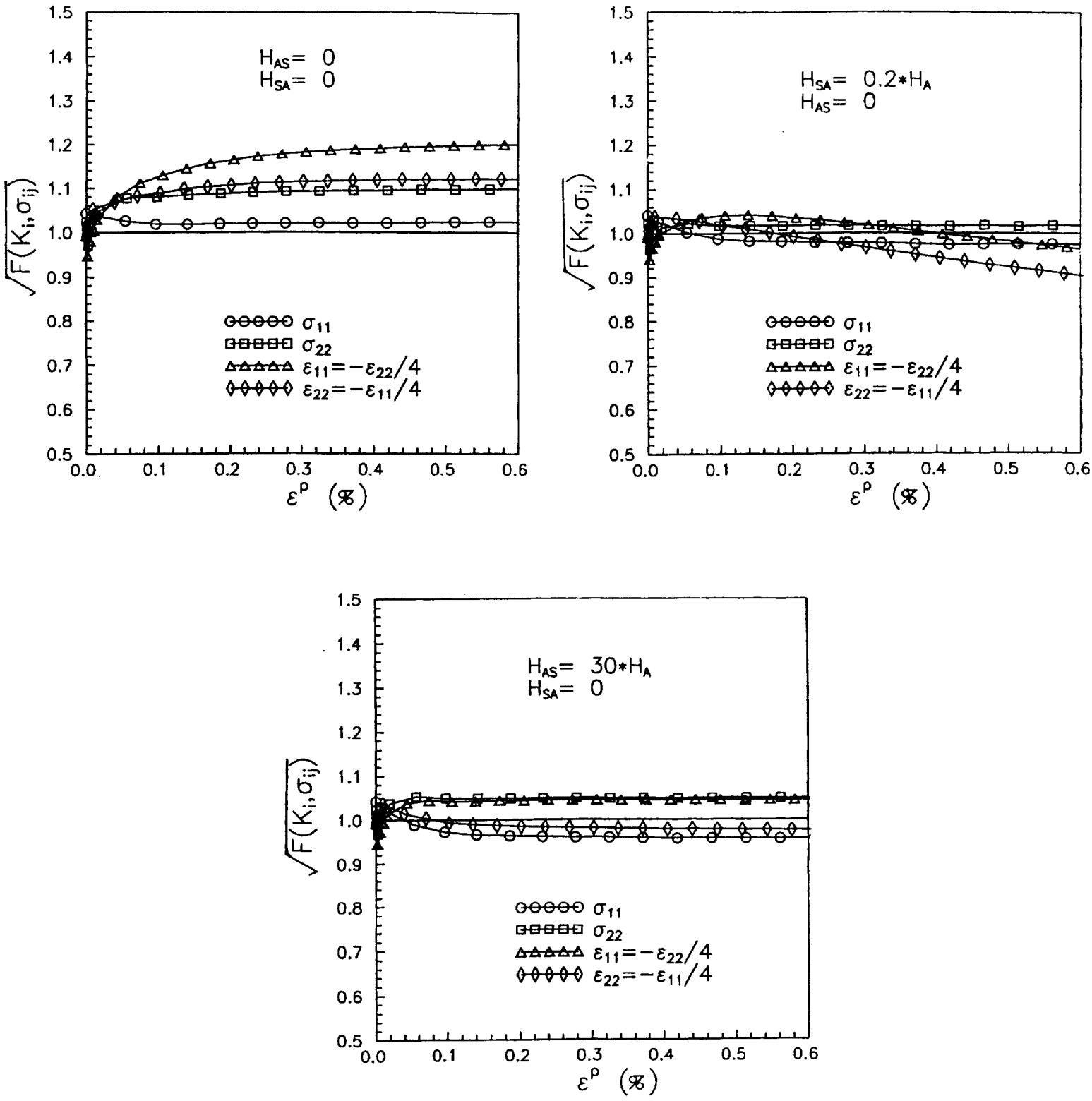

Fig. 11 Influence of cross hardening terms on the value of the flow-potential for transverse loading.

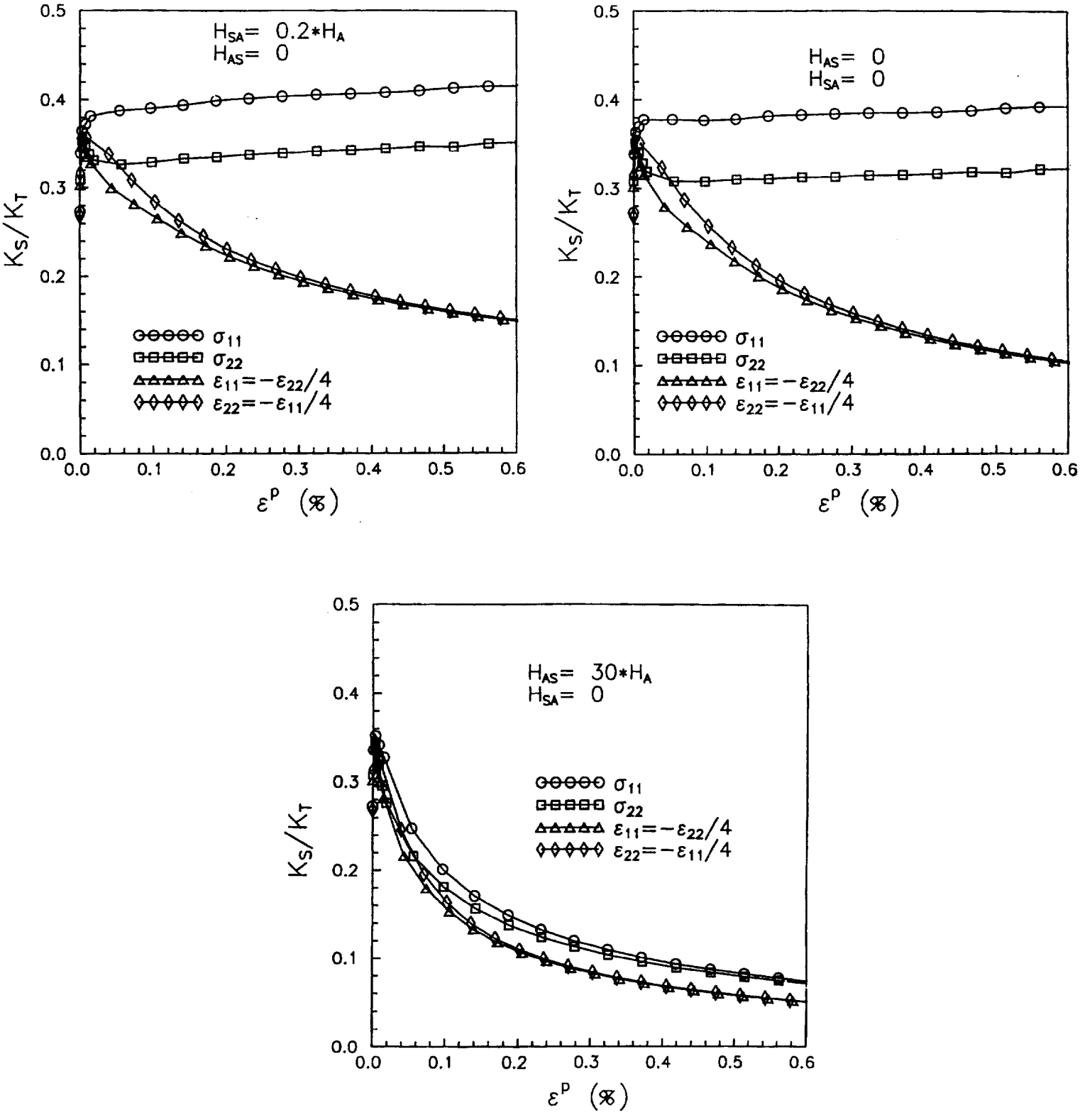

Fig. 12 Influence of cross hardening terms on the ratio of yield stress in shear to yield stress in transverse biaxial tension for transverse loading.